IEEE Access
Multidisciplinary ⋮ Rapid Review ⋮ Open Access Journal

Received 22 September 2022, accepted 5 December 2022, date of publication 15 December 2022,
date of current version 28 December 2022.

Digital Object Identifier 10.1109/ACCESS.2022.3229588

RESEARCH ARTICLE

Sectors, Beams and Environmental Impact on the Performance of Commercial 5G mmWave Cells: An Empirical Study

SALMAN MOHEBI[1], (Member, IEEE), FOIVOS MICHELINAKIS[2], (Member, IEEE), AHMED ELMOKASHFI[2], (Member, IEEE), OLE GRØNDALEN[3], KASHIF MAHMOOD[3], AND ANDREA ZANELLA[1], (Senior Member, IEEE)

[1]Department of Information Engineering, University of Padova, 35131 Padova, Italy
[2]Simula Metropolitan, 0167 Oslo, Norway
[3]Telenor Research, 1360 Fornebu, Norway

Corresponding author: Salman Mohebi (mohebi@dei.unipd.it)

This work was supported in part by the European Community through the 5G-VINNI Project within the H2020-ICT-17-2017 Research and Innovation Program under Grant 815279, and in part by the European Union's Horizon 2020 Research and Innovation Program under the Marie Skłodowska-Curie Grant under Agreement 813999.

ABSTRACT millimeter wave (mmWave) communication is one of the cornerstones of future generations of mobile networks. While the performance of mmWave links has been thoroughly investigated by simulations and testbeds, the behavior of this technology in real-world commercial setups has not yet been thoroughly documented. In this paper, we address this gap and present the results of an empirical study to determine the actual performance of a commercial 5G mmWave cell through on-field measurements. We evaluate the signal and beam coverage map of an operational network as well as the end-to-end communication performance of a 5G mmWave connection, considering various scenarios, including human body blockage effects, foliage-caused and rain-induced attenuation, and water surface effects. To the best of our knowledge, this paper is the first to report on a commercial deployment while not treating the radio as a black box. Measurement results are compared with 3GPP's statistical channel models for mmWave to check the possible gaps between simulated and actual performance. This measurement analysis provides valuable information for researchers and 5G verticals to fully understand how a 5G mmWave commercial access network operates in the real-world.

INDEX TERMS 5G, commercial 5G networks, coverage analysis, millimeter-wave, mmWave.

I. INTRODUCTION

The abundant free spectrum available at millimeter wave (mmWave) frequencies, spanning from 30 GHz to 300 GHz, makes mmWave communication a key enabler for 5th Generation (5G) systems to support bandwidth-hungry applications like online High Definition video streaming, augmented and virtual reality, and road-side vehicular communications.

However, transmission over mmWave bands has its unique characteristics and adds new challenges, which are very different from those of sub-6 GHz communications. In the last decade, a massive body of research has been carried out to understand and model mmWaves' propagation properties, mainly focusing on path-loss models, ray propagation mechanisms, material penetration, and atmospheric effects.

The first commercial 5G mmWave systems have already been deployed in the last two years, and some early measurements [1], [2], [3] investigated the performance of these systems under various urban scenarios, revealing a high variability in the systems' performance, partially attributed to the high sensitivity to the propagation environment. These studies are important because commercial installation may require adaptations and parameter settings that were not required or tested in Proof of Concept (PoC) or pre-deployment phases and that may potentially affect the system behavior in certain situations. Evidence of such a risk was

The associate editor coordinating the review of this manuscript and approving it for publication was Young Jin Chun.

reported, for example, in [4] where the authors observed that an unexpected setting of some base station parameters had a dramatic impact on the energy consumption of narrowband-IoT nodes, significantly deviating from what was predicted by models based on the protocol specifications. So, further research is required to fully understand the behavior of mmWaves in an operational setup. To this end, we have conducted a measurement campaign to analyze the impact of different environmental phenomena like rain, water surfaces, foliage, and human body blockage on the performance of an operational 5G mmWave cell. We have also studied the signal coverage in different propagation environments for different sectors and beams. The purpose of this study is hence to understand to what extent the expected performance of mmWaves is fulfilled in commercial settings, with all the complexity of an actual cellular system and of a real-world environment. In many cases, our results confirm the system behavior already observed in previous studies based on non-commercial PoC deployments or predicted by theoretical models and simulations. However, in a few cases, we observed some nonconforming results that may predict problems in commercial deployment.

The analysis of the measurement results provides guidelines for planning future deployments and predicting the performance of 5G in different use cases, such as in fish farms/aquaculture [5], when the User Equipment (UE) is located inside forests or vegetated areas [6], or when the Line-of-Sight (LoS) signal is blocked by buildings, moving objects or humans, as in dense urban environments [7]. Therefore, our observations are especially helpful to industries interested in deploying 5G over mmWave frequencies, but are not familiar with its intricacies.

In summary, our main contributions are as follows:

- We present the coverage analysis of a commercial 5G mmWave cell by measuring the Reference Signal Received Power (RSRP) in a complex real-world propagation environment (Section IV-A).
- We then analyze the beam separation and gauge the difference with respect to the sector-level transmission (Section IV-B).
- We study different environmental impacts from the body and foliage blockage to rain and over-water transmission on mmWave links on the commercial setup (Section IV-C).
- We analyze the performance of Non-Line-of-Sight (nLoS) mmWave links in two different sectors, representing urban and suburban areas, observing that in an urban environment with multiple buildings and reflecting elements, the nLoS components of mmWave signals can compensate for the lack of LoS links, while this is not the case in the suburban environment (Section IV-C).
- We analyze the effect of the above-mentioned scenarios on the performance of end-to-end transmissions (Section IV-C).
- We compare the measurement results with 3rd Generation Partnership Project (3GPP)'s statistical channel models for the urban and rural environment both for omnidirectional RSRP and transceiver's optimal antenna configuration, revealing the gap between the ideal simulated environment and the complex propagation environment (Section V).
- Finally, we discuss how the above would affect real-world applications (Section VII).

The remainder of this paper is structured as follows: Section II reviews the existing literature around mmWave propagation and early 5G mmWave deployments. Section III describes the methodology used to conduct the measurement campaign. The observations and result analysis is provided in Section IV, and Section V compares the measurement results with some simple simulated scenarios. Section VI summarizes key findings and take-home messages and finally, Section VII concludes the paper.

II. RELATED WORK

In the past few years, several studies have experimentally investigated the behavior of mmWave propagation in different scenarios and conditions: indoors [8], [9], [10]; urban environments [11], [12], [13]; suburban and vegetated areas [14], [15], [16]; human body blockage [17], [18] and rain-induced fading [19], [20]. Further, [21], [22], [23], [24], [25], [26] study end-to-end transmissions over mmWaves. Table 1 presents a summary of the related work.

The studies mainly aim to characterize the propagation of mmWave signals in different environments and under various circumstances. For example, the measurement study in [11] considered outdoor 32 GHz microcells to extract and develop a mmWave channel model. The empirical result was then compared and validated through simulation. Ko et al. [12] investigated the wideband directional channel characteristic of mmWaves in both indoor and urban environments to model the spatio-temporal features of the communication channel. In [13], the authors performed a measurement study to investigate the feasibility of mobility for a typical vehicular speed in the urban environment.

The propagation of mmWaves in suburban and vegetated environments, which contain lots of foliage, is highly different from the urban and indoor scenarios. This matter has already been considered in the literature, where a vast body of research studies the effects of foliage attenuation on mmWave propagation. A measurement study in [14] analyzed and extracted large-scale and small-scale propagation properties of 5G mmWaves in various vegetated environments with different types and densities of vegetation. A real-time channel sounder was used in [15] to measure mmWave LoS and nLoS channel responses in a suburban area with lined trees. The authors then used the measurement results to generate a foliage propagation model based on the ITU-R terrestrial model.

The propagation of mmWaves can also be highly affected by different phenomena like rain and human body blockage. 3GPP has recognized human body as one of the main obstacles affecting mmWave propagation and causing large

TABLE 1. Related works.

Ref.	Year	Scenario	Methodology	Contribution
[1]	2020	5G urban	Measurement (commercial)	Performance of end-to-end transmission in different scenarios
[2]	2021	5G urban	Measurement (commercial)	Performance, power consumption, and application QoS
[3]	2020	5G urban	Measurement (commercial)	Factors affect 5G performance in UE-side
[8]	2020	LoS indoor corridor	Measurement (testbed)	Path loss model
[9]	2018	LoS indoor office	Measurement (testbed)	Path loss/ Large scale fading
[10]	2019	LoS/nLoS indoor lecture hall	Measurement (testbed)	mmWaves channel characteristics
[11]	2017	Urban	Simulation/Measurement	Channel modeling
[12]	2017	Urban/Indoor	Measurement (testbed)	Spatio-temporal features of channel
[13]	2018	Urban	Measurement (testbed)	Feasibility of mobility
[14]	2020	Foliage/Suburb	Measurement (testbed)	Propagation characterization
[15]	2017	Foliage/Suburb	Measurement (testbed)	Propagation characterization
[16]	2017	Foliage/Suburb	Measurement (testbed)	Foliage propagation model
[17]	2019	Body blockage	Measurement (testbed)	Human blockage model
[18]	2019	Body blockage	Simulation	Hand grip impact
[19]	2019	Rain	Measurement (testbed)	Rain attenuation
[20]	2020	Rain	Measurement (testbed)	Rain attenuation
[21], [22]	2020	End-to-end urban	Simulation	Performance of TCP in mmWave
[23], [24]	2017	End-to-end urban	Simulation	Performance of TCP in mmWave
[25]	2019	High speed/Urban/Indoor	Simulation	Performance of TCP in mmWave

radio channel variations. Human body blockage has been considered and modeled in the literature, based on Double Knife Edge Diffraction (DKED), wedge, and cylinder models [27]. In [17], human body blockage is measured at 15 GHz, 28 GHz, and 60 GHz for 15 humans with different heights and weights. They model the body blockage as a Double-truncated Multiple Knife-edge (DTMKE) scheme and compare the calculated diffraction with existing models such as the absorbing double knife-edge model and the 3GPP human blockage model.

The attenuation caused by precipitation can not be neglected at mmWave bands, where rain droplets can absorb mmWave signals whose wavelengths (1 mm to 10 mm) is comparable to the size of a raindrop (a few millimeters). Rain attenuation in the 21.8 GHz and 73.5 GHz bands, based on a one-year measurement campaign in tropical regions, is presented in [20]. In Huang et al. [19] employ a custom-designed channel sounder for 25.84 GHz and 77.52 GHz frequencies to measure the rain-induced signal attenuation for short-range mmWave links.

From the user experience perspective, the efficiency of end-to-end transmission is critical when mmWave links are part of the network, as the unsteady physical channel makes it difficult to support higher-layer connections. In Poorzare et al., [21], [22] presented an analysis of reliable end-to-end communications in 5G networks by investigating the effects of mmWave on Transmission Control Protocol (TCP) performance and discussed the factors impacting the performance of 5G networks. They further evaluated the performance of TCP in urban environments under different conditions. Polese et al. evaluated the performance of TCP over mmWave links, relying on simulation [23], [24]. They studied the behavior of multipath-TCP on 28 GHz mmWave links with a secondary Long Term Evolution (LTE) or 73 GHz mmWave link. Zhang et al. [25], analyzed the performance of TCP in mmWave networks for high-speed UEs in dense urban environments, where the UE is located at different geographical positions with LoS and nLoS links to the Base Station (BS) as well as indoor UE. They studied the performance of edge and remote servers as well as different TCP variations.

Most of the previous works were conducted in test setups that were not equipped with commercial 5G mmWave BSs since commercial mmWave deployments did not arrive until late 2019. Notable exceptions are studies by Narayanan et al. [1], [2], and [3]. The study [1] presents a first look at the performance of two mmWave and one mid-band commercial 5G deployments in US. Using end-to-end performance measurements, Narayanan et al. tracked the interplay between propagation in the urban environment, blockage, and precipitation on applications performance. They further expand their measurement campaign in [2] to include power consumption and application Quality of Experience (QoE) of operational 5G networks by considering different deployment schemes, radio frequencies, protocol configurations, mobility patterns and upper-layer applications. They also investigate the possibility of predicting network throughput in commercial mmWave 5G networks [3]. That work identified the different factors that affect 5G performance and proposed a context-aware throughput prediction framework based on Machine Learning techniques.

Like the work of Narayanan et al., we present an evaluation of a commercial 5G cell deployment. However, to the best of our knowledge, this paper is the first to provide a fine-grained analysis of mmWave propagation of a commercially deployed BS. This offers concrete explanations for the main causes of performance degradation since we are not treating the radio as a black box. We have also investigated a range of scenarios that are known to impact mmWave propagation, including human body blockage, foliage, transmission over-water and rain. While some of these have been investigated before, this paper is the first to analyze all of them in a commercial 5G mmWave deployment with known parameter configurations. We also note that this paper is the first to

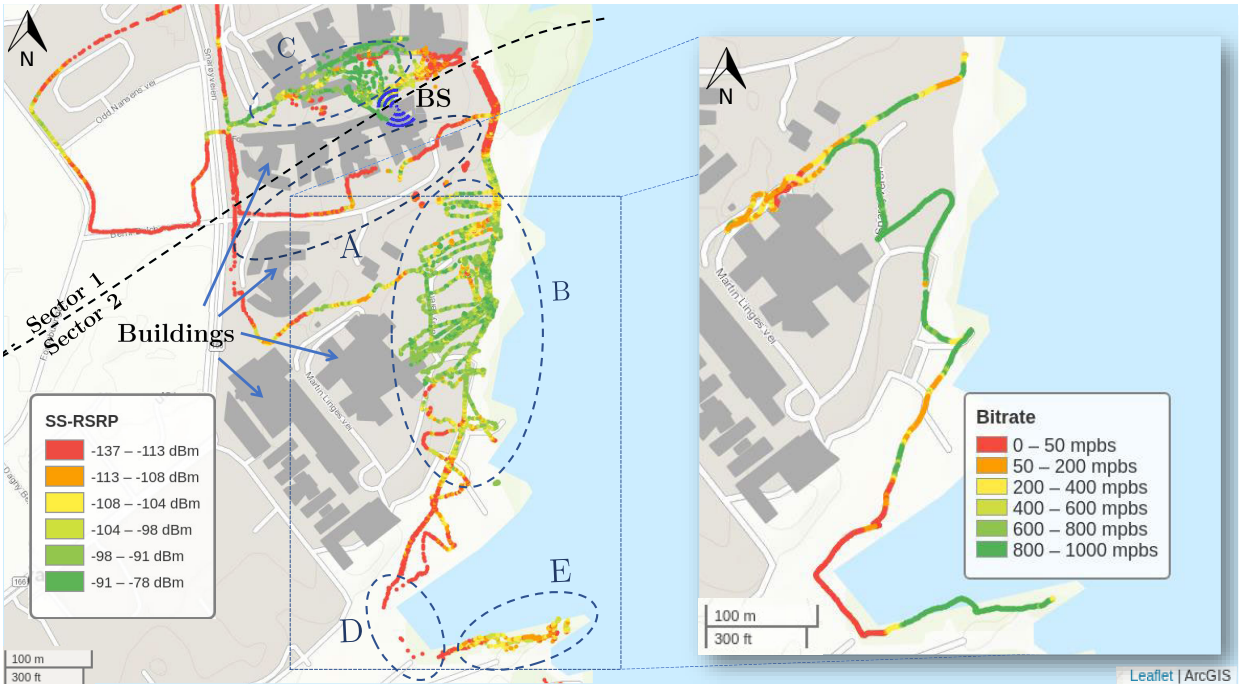

FIGURE 1. Signal coverage map of the cell site, showing the maximum RSRP among all beams and PCIs. The zoomed-in area presents the bitrate.

look at the effect of transmission over-water. We further compare the measured RSRP against 3GPP's statistical mmWave channel models for the urban and rural environments, considering both omnidirectional and strongest RSRP (transceiver's optimal antenna configuration), to study the simulation and actual performance (Section V).

III. MEASUREMENT METHODOLOGY

This paper includes two measurement studies: the first study aims to analyze the coverage aspects of commercial 5G mmWave cells, while the second study targets the end-to-end communication performance of a 5G network when mmWave links are employed as part of the system.

The 5G mmWave BS is located on the roof of a 15 meters high building in Telenor's campus in Oslo, Norway. The BS is equipped with two Huawei HAAU5213 radio frequency units with 768 antenna arrays providing coverage to a northern and a southern sector as shown in Figure 1. Its frequency range is 26.5 GHz to 29.5 GHz with a maximum transmit power equal to 32.5 dBm. It supports up to four carriers and can generate 16 different static beams, employing hybrid beamforming. The black dashed line in the Figure 1 showcases the topological separation of the two sectors. The northern sector (sector 1) points towards an open square surrounded by glass and steel buildings. The southern sector (sector 2) is directed towards a peninsula with some buildings on the west and sea on the east. Each sector has four 200 MHz wide channels (800 MHz total), with center frequencies between 26.6 GHz and 27.2 GHz. We identify each channel by its respective Physical Cell Identity (PCI), where PCIs 101-104 and 301-304 belong to the northern and southern sectors respectively. The operator can adjust the beams' boresight both in the horizontal and vertical plane. We did not have any control of the beams and no prior knowledge about their directions. However, we were able to estimate the beams' directions based on the measurements we collected to create the coverage map from LoS scenarios. If a single beam has the highest RSRP in all locations of a measured area, it is considered to have an orientation towards this area.

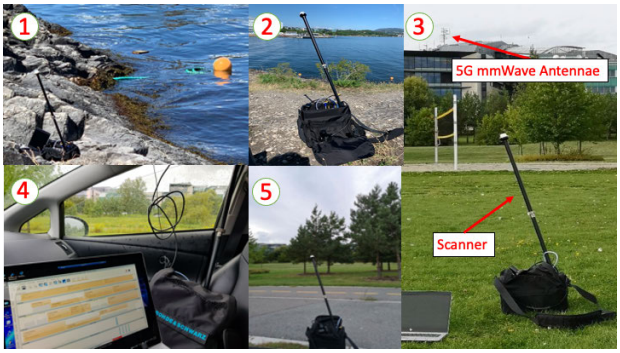

FIGURE 2. Some measurement locations: 1) close to water, 2) 6 m above water, 3) Line of Sight, 4) rain, 5) foliage blockage.

We collect channel quality information with a Rohde & Schwarz scanner [28] that can monitor all the relevant channels simultaneously using an omnidirectional antenna. Note that our measurements do not consider the antenna gain that is expected in a commercial receiver (e.g., as smartphone). On the other hand, the isotropic antenna makes the

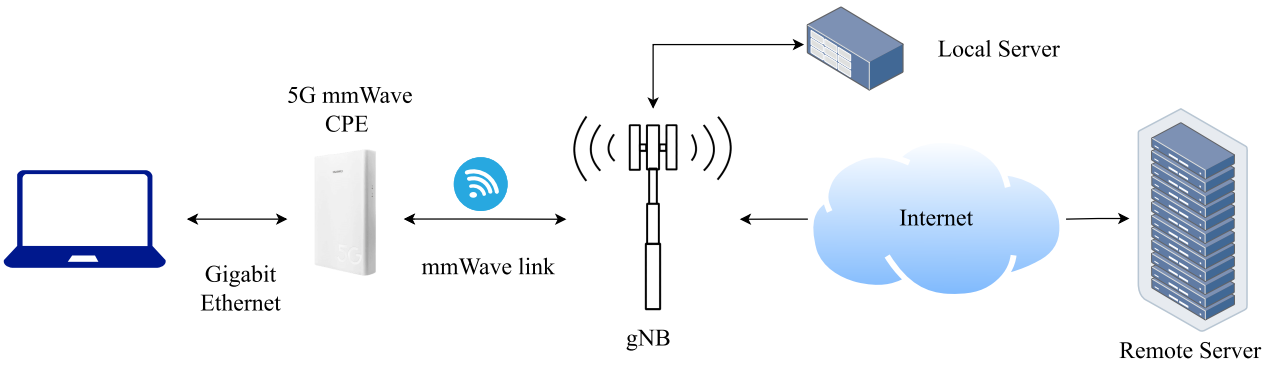

FIGURE 3. Measurement setup for the end-to-end communication experiment. The CPE is connected through a Gigabit Ethernet cable to a laptop running the scripts.

measurements almost independent of the receiver orientation. Since we are interested in how different factors affect propagation, the absence of the receiver gain does not influence our evaluation. The scanner was used to gather measurements across the site and under different conditions, collecting in total 535,137 samples between April 2020 and September 2020. Each sample contains several channel quality indicators, such as RSRP, for all the detected PCIs and beams. We create a coverage map by walking around the site with the scanner, and perform stationary measurements at selected locations, each lasting typically at least 5 minutes, to capture the time variations of the signal strength. Figure 2 shows the scanner and some of the measurement scenarios.

We also performed measurements to analyze the behavior of 5G mmWave end-to-end transmission. Because of BS maintenance, the northern sector was not operational, so the measurements for the bitrate and delay study were done only in the southern sector. Each experiment was repeated at exactly the same locations and with the same BS configuration used for the channel quality measurements. This experiment focused on the user experience, so we evaluated the end-to-end bitrate and Round Trip Time (RTT). The measurements were performed with a pre-production Huawei 5G CPE, supporting 2 × 2 MIMO and operating in Non Standalone (NSA) mode. A Gigabit Ethernet cable connected the CPE to a laptop which acted as the client. Even though the BS can achieve approximately 3 Gbps in downlink, the Gigabit Ethernet limited the maximum transfer rate with the laptop to 1 Gbps. This did not pose an obstacle for our analysis, since we were only interested in the cases where the network performance drops well below this limit as a consequence of obstacles or other environmental phenomena. Figure 3 shows the measurement setup used for this study.

The traffic sources were servers located inside the operator's network to avoid the effect of cross-traffic and congestion over the public Internet. The delay performance was assessed from the RTT measurements given by `ping`, with packets of 64 bytes (default setting) and of 1500 bytes (maximum size allowed by the Ethernet connection without requiring IP fragmentation). Note that, to be transmitted over the wireless link, the bigger `ping` packets have to be split into multiple Transport Blocks when the system experiences bad signal, which results in the use of robust (but not very spectrum efficient) modulation and coding schemes. The bitrate performance was evaluated through `iPerf3`,[1] a cross-platform tool for network performance measurement. We used ten parallel TCP connections, lasting at least 10 seconds, to get an estimation of the bitrate achieved at each measurement location.

IV. MEASUREMENT RESULTS

A. COVERAGE ANALYSIS

We first focus our analysis on the measured Synchronization Signal Reference Signal Received Power (SS-RSRP), which is the average power of the Resource Elements (REs) that carry the Secondary Synchronization Signal (SSS) transmitted within a Synchronization Signal Block (SSB) [29]. The beams are time-multiplexed, thus there is no interference between the beams when the SS-RSRP is measured. For simplicity, we will refer to SS-RSRP as RSRP. Each SSB/beam is assigned a unique number, called SSB index. Note that the values of the SSB index are not contiguous. Thus, in the subsequent plots, the numbering of SSB indexes has gaps.

Figure 1 presents the mmWave coverage map. At each location, we were able to detect all the PCIs of the relevant sector and most of the beams. Since a UE would be attached to the dominant beam, i.e., that with the highest RSRP among those detected by the UE, in Figure 1 we report only this maximum RSRP values.

In mmWave bands, the RSRP is dominated by the signal's LoS components: missing these components can lead to significant attenuation. This can be easily seen in area **A** of Figure 1, where the LoS link is blocked by buildings and the RSRP drops below −113 dBm. Although the availability of LoS components of a mmWave signal is an important factor in determining coverage, other effects like signal

[1] https://iperf.fr/

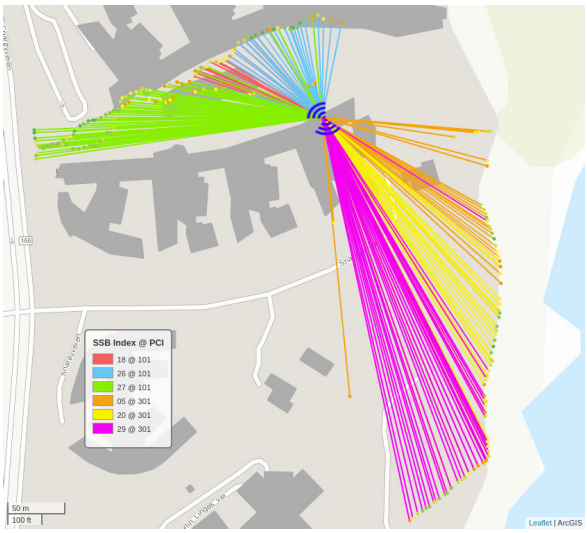

FIGURE 4. Dominant beams (lines) and the related RSRP values (points) in a subset of the locations.

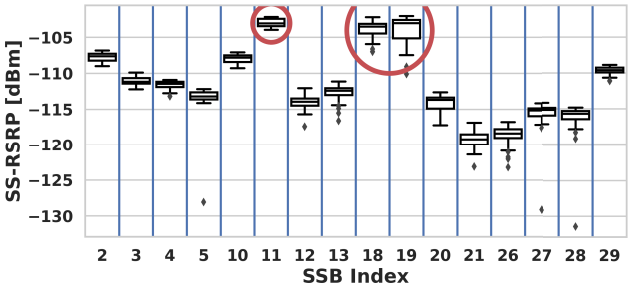

FIGURE 5. On rare occasions, we observe multiple dominant beams. Static measurements over a 5-minute period at a location 250 m away from the BS, where several beams could be considered dominant (highlighted with red circles).

diffraction, reflections from surrounding objects, and multipath propagation can compensate for their absence. These effects are likely responsible for the relatively large RSRP measured in Area **C** of sector 1, between the two buildings, where the LoS link is blocked by the roof edge of the building hosting the BS. In contrast, in absence of reflecting or diffracting elements, there are no nLoS components of mmWave signals. This is the case of area **A**, where the signal propagates in a vegetated area without many reflecting elements, and of area **D**, where we did not record any significant RSRP value at most of the locations.

As expected, we did not observe a significant difference between PCIs for the same beam. Moreover, in presence of LoS, we did not record a strong dependency between signal power and distance to the BS. The attenuation due to the increasing distance is indeed marginal compared to the rest of the factors that affect the RSRP, which fluctuates within a certain range as long as the receiver remains in the main lobe of the dominant beam. This behavior can be observed by considering a straight LoS line in Area **B** and sampling locations at a distance from the BS ranging from 200 m to 450 m. At such LoS locations, the median RSRP value of the dominant beam is always between -94 dBm and -100 dBm, regardless of the distance. We hypothesize that it is the vertical antenna gain pattern that is causing this behavior. At short distances we were located significantly below the boresight of the BS antenna, hence the antenna gain was low. As we moved further away we got closer to the boresight and the antenna gain increased. So the effects of larger pathloss and increasing antenna gain as the distance increased approximately cancelled each other. We discuss in more detail the relationship between RSRP and distance in Section V, where fig 11b illustrates our measurements and compares the maximum measured RSRP to state of the art models.

To construct the bitrate map, we launched 10 parallel continuous TCP connections and walked around the cell site with normal speed, while tracking the location by external GPS. Simultaneously, `tcpdump` captured the generated traffic. We generated an estimate of the observed bitrate at each location by correlating the timestamps of the packet capture and the GPS log. The packet capture was split into 100 ms bins and all the packets received during a bin were grouped together. The bandwidth values were estimated by dividing the total number of bytes of all the packets in a bin by 100 ms. Then, we assigned this bandwidth value to the closest, by time, GPS entry. As shown in Figure 1, the bitrate in different locations is highly correlated with the RSRP: the higher the RSRP, the higher the bitrate. As seen in the figure, in the LoS locations, the maximum possible bitrate is achieved. Even in area **E**, which is relatively far from the BS, the bitrate is high. Note that, the Gigabit Ethernet connecting the CPE to the Laptop is the bottleneck and limits the network speed to 1 Gbps. In a very bad channel state (area **D**), TCP still keeps the connection open but with a very low bitrate.

B. BEAM SEPARATION

A sharper beam can increase MU-MIMO performance by improving spatial separation between users, and can reduce interference in multi-cell deployments. To showcase beam separation, we selected a few locations, creating a perimeter at the ground level around the BS. Figure 4 color codes the dominant beam at each location. The beam lines drawn on the map are hypothetical, connecting the BS and receiver location. The actual beams are not as narrow as we have shown in the figure: signals from different beams can be detected at a much wider angle (side lobes) and even at the backside of the transmitter (back lobes). According to [30], the RSRP should be above -110 dBm to be detectable by 5G NR UEs, thus we filter out values below this threshold. For each sector, we have also displayed only three out of 16 beams and have not considered the beams that overlap in the vertical plane. We observe a similar beam separation pattern across the vertical axis, by performing measurements on several floors at the building opposite of the BS at sector 1.

TABLE 2. Summary of the body blockage effect on bitrate.

Position	Bitrate [Mbps]
Line of sight	822
No line of sight (2 sitting 2 meters away from the CPE)	613
No line of sight (2 standing right in front of the CPE)	755

The dominant beams at the ground level, third floor, fourth floor and roof are different.

As commented in Section IV-A, within a certain range, the actual distance between transmitter and receiver is not of much relevance as long as the receiver is within the main lobe of the dominant beam. Therefore, it is possible to get good signal even at long distances. The furthest point from the BS we could detect RSRP higher than −110 dBm was 902 meters. We can assume commercial UEs would be able to achieve an even bigger range, because of the receiver antenna gain. At almost all the studied locations, a single beam had consistently and markedly higher RSRP than the rest for the whole measurement duration, so beam selection was trivial. However, it is possible to have multiple dominant beams in some locations, as shown in Figure 5, where the RSRP values for different beams are presented at a single location for one PCI over a 5 minute period. We observe that three beams, marked with red circles, have about the same median value. The number of simultaneous beams is limited by the number of Transmit/Receive (transceiver) units in the BS, so only one beam is transmitted in any given time/frequency slot for each PCI. This time multiplexing avoids inter-beam interference, but beam selection becomes more complicated. In such cases, it might be better to have a secondary criterion for beam selection, such as choosing the beam with the lowest standard deviation of RSRP. Even more sophisticated beam selection algorithms [31], [32] might be required in a more complicated and dynamic propagation environment. On the other hand, the slightly overlapped coverage regions of the SSB beams are good for robustness (body blockage, moving cars, etc), where there is a higher chance of having at least a good beam at any time. The other benefit of this slight overlap (or closely spaced beams) is to have a smooth user experience as a UE moves from one beam's coverage region to another beam's.

C. ENVIRONMENTAL IMPACT ON MMWAVE PROPAGATION

In the following, we analyze the effect of different environmental factors such as human body blockage, communication over-water surfaces, foliage and rain-induced attenuation on mmWave propagation.

1) HUMAN BODY BLOCKAGE EFFECTS

To analyze the impact of human body blockage, we placed the scanner at a LoS location 260 meters away from the BS. We then blocked the direct link from the BS in two different ways. First, by standing 10 cm away from the scanner,

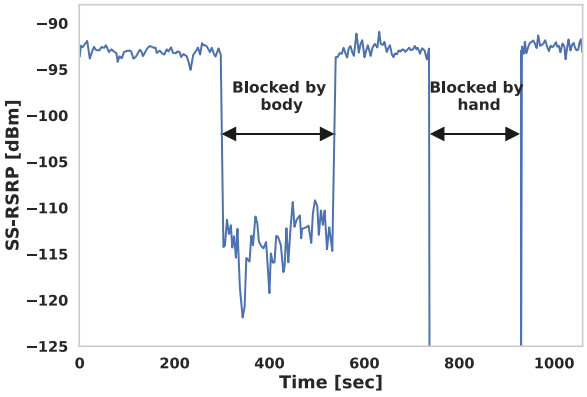

FIGURE 6. Body blockage effect on mmWave propagation at a location 260 m away from the BS with a LoS link.

TABLE 3. Summary of the effect of different types of foliage to bitrate and delay.

Position	Bitrate [Mbps]	RTT [ms]	RTT big [ms]
LoS baseline besides the trees	891	14.6	15.7
Beside a small tree	831	13.4	16.6
Behind a single branch	785	14.8	17.5
Behind a big tree with sparse leaves	451	14.8	19.6
Behind a big tree	323	15	17.8

and later by folding a hand around the scanner's antenna, which are typical behaviors of smartphone users. As shown in Figure 6, we observed a 20-30 dB drop in RSRP in the first experiment, which is in line with the literature [18]. In the latter case, all the signal components were removed, and we were unable to detect any signal. In the first case, the received signal was likely due to the nLoS components reflected or scattered from the surrounding objects, or diffracted from the person standing in front of the scanner. Folding a hand around the scanner's antenna, instead, completely shielded the receiver from all the signal components, which explains the absence of significant RSRP measurements. The human body blockage effects on mmWave communications have already been investigated and modeled in various ways, and the interested readers can refer to [17] and [33] for more information. Our experiments hence confirm this critical aspect also in commercial cell deployments.

The effect of body blockage on bitrate is presented in Table 2. We measured the bitrate with 10-parallel TCP connections as above, while 1) two average-size people were sitting about 2 meters away from the CPE, completely covering the LoS link, and 2) two people standing right in front of the CPE. As seen in the table, the bitrate dropped from 822 Mbps to about 613 Mbps and 755 Mbps for the first and second scenarios, respectively. This shows that despite the partial occlusion of LoS, the performance at the TCP layer seems to remain acceptable.

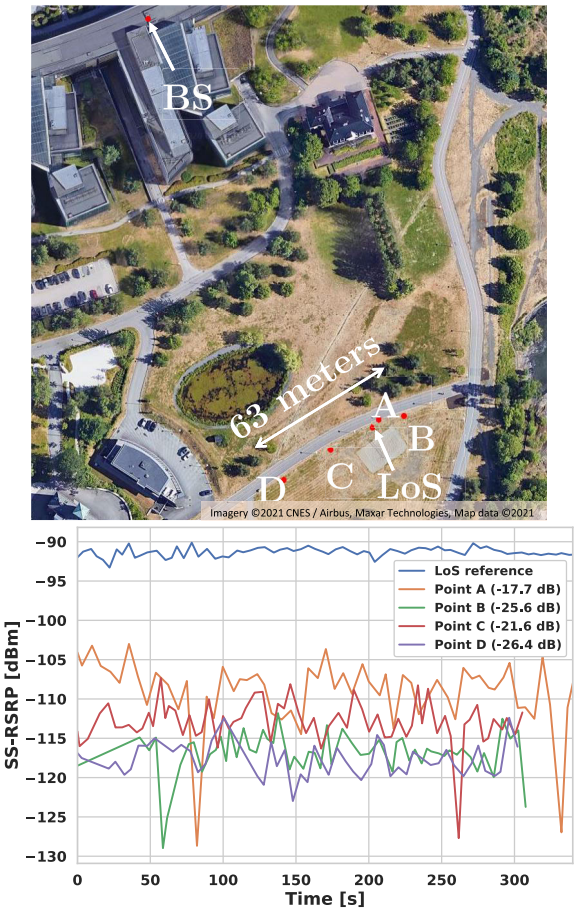

FIGURE 7. Foliage attenuation scenarios compared to LoS. Locations A, B, C and D suffer from different types of foliage blockage. Distance from BS: ≈220 m for all locations.

2) FOLIAGE ATTENUATION

The propagation characteristics of mmWave frequencies in suburban and vegetated environments are very different from those in urban and indoor scenarios. Foliage attenuation could significantly affect communication over this frequency range and should be considered in network planning for such suburban areas [14]. We carried out a set of measurements to investigate the effect of blocking the path between transmitter and receiver by trees and other vegetation. During the measurements, nearby weather stations reported wind intensity between 4.7 and 5.9 m/s, which is considered a "gentle breeze" according to the Beaufort scale. The leaves and twigs on small trees were in constant motion.

Figure 7 shows the RSRP at 4 different locations where the LoS path is blocked by different types of trees. The high variation in RSRP is likely due to wind that constantly moved tree branches and leaves, which resulted in varying blockage and reflection patterns. The recorded RSRP exhibits significant attenuation at all four locations, typically 15 dB to 30 dB lower than our measurements at a nearby reference LoS location. The intensity of attenuation highly depends on the type and shape of the blocking trees, with bigger trees causing higher attenuation. As Figure 7 illustrates, the smaller trees at location **A** attenuate the signal by 17.7 dB, while the bigger ones at location **D** decrease the received signal power by up to 26.4 dB. This result is comparable with similar studies, where the authors reported 22.48 ± 0.92 dB foliage attenuation in 26.5 GHz [34].

Table 3 summarizes the result for the foliage effect on bitrate and delay. The measurements take place another day, under a gentle breeze (wind speed between 2.4 to 5.1 m/s). As was expected, the bitrate drop and delay are highly correlated with the result from the RSRP measurements. The bigger trees with more dense branches and leaves cause a more significant drop in RSRP, and these unreliable links result in decreasing the bitrate and increasing the RTT. Based on the type of foliage and tree, communication speed dropped from 891 Mbps at the LoS baseline location to 426 Mbps when measured behind small trees and further dropped to 323 Mbps behind big trees. Also, the delay is larger for big packets than for small packets, as they may break into multiple Transmission Blocks and be retransmitted multiple times under challenging signal conditions.

3) RAIN-CAUSED ATTENUATION

We collected measurements on two different days, with dry and rainy weather, at the same location. During the rainy day, nearby weather stations reported precipitation between 0.1 and 0.2 mm per minute, which is a moderate to heavy rain intensity. Figure 8 presents the RSRP values measured for different weather conditions for a single PCI, grouped per beam. Results for the other PCIs are similar. As it can be seen from the figure, rain causes a notable drop in the mean RSRP and increases its variability in particular for the weaker beams.

The increased variability for the weaker beams is probably caused by multi-path signal propagation where no single signal component is significantly stronger than all others. The most significant components will consist of signals reflected by e.g. buildings and vegetation, and usually also of the LoS signal. Strong beams point towards the scanner and the BS antenna gain for the LoS signal will be high. Therefore the LoS signal will be much stronger than the reflected signals, and the received signal power will have little variability. Weak beams, on the other hand, do not point directly towards the scanner and the BS antenna gain for the LoS signal is therefore low. In this case the strength of the reflected beams might be comparable to or larger than the strength of the LoS component. This results in multi-path fading that gives large variability in the received signal power.

4) OVER-WATER COMMUNICATION

We also investigate how water surface scattering and reflection affect mmWave signals. This scenario could be relevant when mmWaves are used for providing high capacity communications on the shore. For example, fish farms plan to use mmWaves for high definition video communications between fish cages and on-land data centers where advanced signal

TABLE 4. Water effect on mmWave propagation, across all the southern sector's PCIs. Instances with high standard deviation are highlighted.

Beam type	Distance (m)	PCI-301		PCI-302		PCI-303		PCI-304		TCP		
		mean [dBm]	std	mean [dBm]	std	mean [dBm]	std	mean [dBm]	std	Bitrate [Mbps]	RTT [ms]	RTT big [ms]
Over water (close to sea level)	792	-103.2	**2.33**	-105.2	**3.12**	-103.7	**2.62**	-105.9	**3.35**	903	13.9	17.5
Over water (6m above sea level)	813	-111.4	**4.61**	-110.6	**4.70**	-107.7	**3.16**	-105.8	**3.25**	885	15.5	16.6
Ground	573	-94.3	0.29	-94.7	0.33	-93.0	0.30	-92.3	0.29			
Ground	256	-103.0	0.54	-102.1	1.21	-100.1	0.66	-100.7	0.76			
Ground	213	-91.3	0.56	-94.2	0.76	-96.4	0.84	-92.2	0.59			
Ground	323	-93.1	0.80	-94.8	1.57	-103.7	**3.20**	-97.5	1.87			

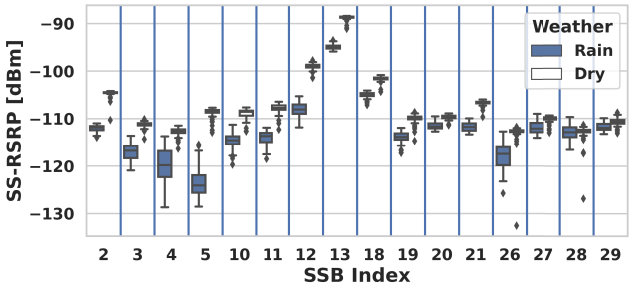

FIGURE 8. Comparison of received power during rain (left element per boxplot pair) and dry weather (right element per boxplot pair) for a single PCI. Distance from BS: 214 meters.

processing and analytics are used to, e.g., control feeding and monitor fish health [5].

We performed the measurements at locations with good LoS of the BS antenna, on the far side of a small bay. From the BS, the mmWave signal first travels over the ground for about 630 meters and then over-water for 160 meters before reaching the scanner. The measurements were collected at two locations. First, we put the scanner at the shoreline about 50 cm from the water. Second, we placed the scanner approximately 6 meters above the water surface. We could not assess the water wave height directly, but during the measurements, nearby weather stations reported a wind intensity between 4.9 m/s and 5.6 m/s, which typically corresponds to wave heights of 0.6 m to 1.2 m. The measurement location is relatively sheltered though, so we can assume that the wave height is closer to the lower limit of this range. For comparison, we also made corresponding measurements at LoS locations with different distances to the BS where the propagation was solely over-ground (due to terrain and building blockage, we were not able to do over-ground propagation measurements at exactly the same distances as for the over-water measures). Table 4 summarizes our measurements. The RSRP standard deviation for over-water propagation is significantly larger than for over-ground propagation. The increased standard deviation for the over-water communications can be explained by a model where the received signal consists of a direct LoS component and one or more components (specularly or diffusely) scattered from the water surface. Since the water surface moves, the scattered components' strength varies with time, thereby causing signal power variations at the receiver.

Another observation from Table 4 is that the difference between the mean RSRP values for PCIs with different frequencies are much larger at 6 meters above the water than at the sea level. This can be explained by the same propagation model. When the scanner is located close to the water surface, the scattered components of the signal are coming from the water immediately in front of the scanner. In contrast, these components are originated much further out when the scanner is placed far above sea level, so the scattered components' delay compared to the LoS is more variable. In frequency domain, this translates to flatter fading (i.e., attenuation is almost the same across neighboring frequencies) when the scanner is at sea level than when placed at a higher location. A consequence of the increased signal variation for over-water reception is that it will be necessary to use a higher link margin in the link budget calculations than when the communication is solely over-ground. The smaller signal variation for the scanner located at sea level suggests that mmWave antennas should be placed close to the water, e.g., on a fish cage.

Table 4 also presents the bitrate and RSRP values for the over-water transmission. The bitrate and the delay at 6 meters above the water are significantly worse than at sea level. This observation was also expected, as the high-level performance is indeed correlated with the RSRP values.

5) nLoS MEASUREMENT SCENARIOS

In mmWave communications, LoS links can be easily blocked by buildings, moving cars and other obstacles. In this case, the RSRP depends on the nLoS components, such as reflected, scattered and diffracted waves. To get an indication of the nLoS coverage, we performed measurements at four locations where the LoS path to the BS antenna was blocked by the roof of the building with the BS (See Figure 9). Locations **S1** and **S2** in Figure 9 are surrounded by high buildings and a large number of rectangular columns placed in a regular pattern in the plaza between the buildings to mimic an urban environment. Locations **S3** and **S4** are surrounded by trees and some distant buildings, representing a suburban and vegetated environment. Figure 10 presents the RSRP distribution of the best beam (written in parenthesis) for every carrier (PCI) of the BS at these locations. Even though the orientation of the beams is the same for all the PCIs at the BS, we observe that at locations **S2** and **S4** the dominant beam is different for some of the PCIs. Further, at location **S2**, PCI

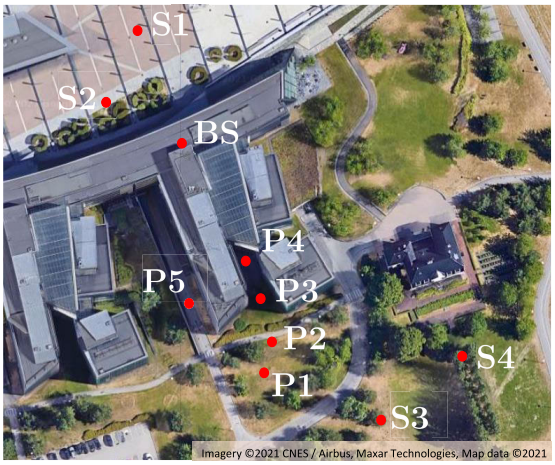

FIGURE 9. Locations where the nLoS measurements were performed.

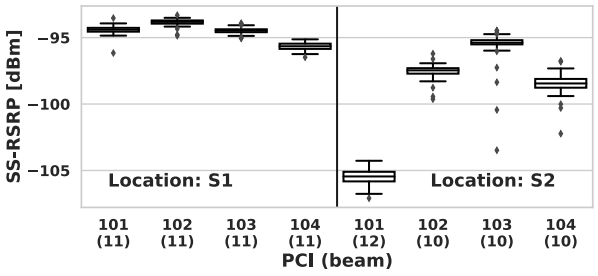

(a) Sector 1 (North)

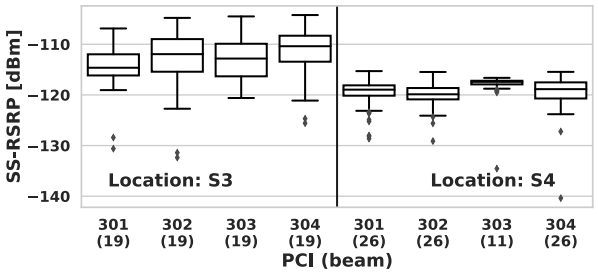

(b) Sector 2 (South)

FIGURE 10. RSRP at different locations with nLoS links. The dominant beam for every PCI is mentioned in parenthesis.

TABLE 5. Summary of the effect of nLoS links to Bitrate and delay.

Position	Bitrate [Mbps]	RTT [ms] normal size	RTT [ms] big size
P1	845	15.4	17.8
P2	573	16.5	33.9
P3	176	15.6	22.1
P4	87	18.0	48.0
P5	177	15.4	18.1

101 has degraded performance compared to the rest of the PCIs. Both observations are in contrast to what we measure at LoS locations. It can be due to the property of different scattering and diffracting materials at different frequencies (i.e., reflection coefficients and penetration losses), but we are unsure about the exact source of these behaviors.

At locations **S1** and **S2** the received signal is quite strong, indicating good nLoS coverage. This is thought to be due to the rich scattering environment, possible reception of diffracted (i.e., from the edge of the roof) signal components and the relatively short distances involved. At locations **S3** and **S4** the received signal level is very low and there is little or no nLoS coverage. This is thought to be due to a much poorer scattering environment. The buildings that might act as good reflectors for the signals are located far away from both the BS antenna and the scanner, hence the signal paths will be very long. The trees in the surrounding area further attenuate both the reflected and the diffracted signal components. These results show that in an urban environment, with multiple buildings and scattering elements, the nLoS components of the mmWave signals could compensate for the lack of a LoS link to the BS. In contrast, in vegetated areas, the LoS link is necessary to establish reliable communication.

Finally, we study the end-to-end communication performance over nLoS 5G mmWave links. To do so, we collect measurements in different locations, close to the buildings, where there is no LoS path to the BS. These locations are marked as **P1**-**P5** in Figure 9. Table 5 reports the bitrate and RTT values for the mentioned locations. It is evident that the bitrate sharply drops and the delay increases by moving toward the buildings. This is an expected observation as fewer diffracted elements reach the locations close to the building, which results in lower RSRP and therefore bitrate.

V. COMPARISON WITH SIMULATIONS

This section compares our measurement results with simulations based on empirical models to check how accurately statistical models can predict the received signal at different locations. The complexity of the propagation environment makes it impossible to use accurate channel models (i.e., ray-tracing based quasi-deterministic channel models [35], [36]) to accurately obtain the nLoS components of the propagated signal. We hence used 3GPP's statistical channel model for mmWave frequencies [37] to estimate the path loss for different scenarios. For Sector 1, we use the Urban Micro (UMi) and Urban Macro (UMa) channel models [38], [39], as the BS is pointed towards a square surrounded by large buildings and the topology is similar to a typical urban environment. Whereas for Sector 2, we employ the Rural Macro (RMa) model [40], as it represents a sub-urban area with more trees and other vegetation and fewer or no buildings. The omnidirectional path loss model used in our simulations is:

$$\mathrm{PL}[dBm](d) = 20\log_{10}\left(\frac{4\pi d_0}{\lambda}\right) + 10n\log_{10}\left(\frac{d}{d_0}\right) + SF, \tag{1}$$

where, d is the distance from transmitter, $\lambda = c/(10^9 f)$ [m] is the wavelength, $c = 3 \times 10^8$ [m/s] is the speed of the light, SF [dB] indicates the shadow fading, whose standard

TABLE 6. Simulation parameters.

Parameter	RMa		UMa		UMi	
	LoS	nLoS	LoS	nLoS	LoS	nLoS
n	2.3	3.1	2	2.9	2	3.2
σ_{SF}	1.7	6.7	4.0	7.0	4.0	7.0

deviation is σ_{SF}, n represents the path loss exponent and $d_0 = 1$ [m] is the free space reference distance. The values for σ_{SF} and n at different scenarios are presented in Table 6.

Figure 11 shows the maximum measured RSRP of the dominant beam at different distances for Sector 1 and Sector 2 and compares it to the RSRP achieved using the omnidirectional path-loss model in (1), as is perceived from two omnidirectional isotropic transmit and receive antennas with 0 dBi gain.

The strongest measured RSRP in Sector 1 is ≈−78 dBm, which is a bit higher than the strongest RSRP in the other sector (≈−84 dBm). As shown in Figure 11a, our measurements can barely fit with the 3GPP UMi and UMa models. The RSRP varies between −78 dBm and and −130 dBm which is always lower than the predicted values by the LoS models and only at larger distance is lower than the nLoS models. This figure clearly shows that statistical channel models are not always capable of predicting the RSRP accurately in every propagation environment. Figure 11b shows that the LoS RMa can estimate the RSRP in locations with clear sight to the BS. Even in Area **E**, where the signal propagates overwater, this model predicts the RSRP relatively well (≤5 dBm error). On the other hand, nLoS RMa fails to accurately predict the RSRP for nLoS locations. The variation in measured power in nLoS is mainly due to changes in the type of the obstacles, scattering objects, and topography of the environment, rather than pure distance. Referring to Figure 1 and Figure 9, the type and shape of obstacles blocking LoS in area **A** and the area between **B** and **D** are very different and composed of buildings with various shape that highly affect the RSRP in these areas.

Table 7 compares the RSRP recorded during the measurement campaign against the 3GPP channel models for both omnidirectional and directional antenna gain patterns at the transmitter and the receiver. To obtain the values for the strongest RSRP, we use the NYUSIM simulator [41], which searches for the best pointing angle among all possible pointing angles employing the specified antenna details (i.e., azimuth and elevations of receiver and transmitter antennas) in both transmitter and receiver. The details of the procedure is out of the scope of the this paper and interested readers may refer to [41] and [42] and the references therein for more details. For this simulation, we assumed that the BS and UE are equipped with 16 and 4 uniform linear array antenna elements, respectively.

As seen in Table 7 and Figure 11, the omnidirectional path loss models only perform well in predicting the mmWave channels in limited LoS scenarios. In complicated environments, especially in nLoS locations with many complex scattering objects, using more advanced ray-tracing-based models is difficult, if not impossible, so some extent of measurement is needed to estimate the RSRP accurately. It is also seen that in the best case, the received power at different locations is as good as the omnidirectional power. The gap between the measurement (and omnidirectional power) and the strongest power is significant for all scenarios (≈50 dBm). This vast gap reveals how much an adaptive dynamic beamformer can improve performance. This specifically makes more sense in some mmWave use-cases where the UEs are stationary, i.e., Fixed Wireless Access (FWA) or do not move fast. Some codebook-based beamforming techniques can be employed for these use-cases where the optimal transmitter/receivers antenna configuration can be learned and saved for future uses.

TABLE 7. Comparing the measured RSRP [dBm] with simulations for different scenarios.

Scenario	Distance [m]	Measurement	Simulation	
			Omni	Strongest
RMa LoS	160	-84.5	-80.8	-31.5
RMa LoS	250	-87.7	-85.2	-36.0
RMa LoS	350	-85.6	-88.8	-39.6
RMa LoS	450	-90.6	-91.4	-42.2
RMa LoS	570	-93.0	-94.0	-44.8
RMa LoS	810	-97.5	-97.7	-48.4
RMa nLoS	80	-103.9	-90.4	-41.2
RMa nLoS	120	-102.7	-93.4	-44.2
RMa nLoS	590	-114.4	-117.6	-68.4
RMa nLoS	690	-120.3	-117.5	-68.3
UMa LoS	60	-79.0	-64.5	-17.2
UMa LoS	160	-88.0	-73.4	-26.1
UMa LoS	250	-88.6	-77.0	-29.6
UMa LoS	500	-97.8	-83.2	-35.9
UMa nLoS	15	-91.6	-63.7	-16.6
UMa nLoS	300	-114.3	-100.5	-53.4
UMa nLoS	450	-123.6	-106.0	-58.8

VI. SUMMARY OF RESULTS AND DISCUSSION

This section summarizes and discusses the results of our measurement campaigns and provides an overview and guidance to the different verticals considering 5G mmWaves communications technology for different use cases.

A. ANALYSIS OF THE STUDY AND DISCUSSION

Based on our measurement results, we can confirm that the range of mmWave cells is strongly affected by obstacles, such as buildings, trees, or human bodies, as already observed in the literature. As expected, the LoS beam is generally the most robust in all situations. The performance of the mmWaves in nLoS environments can be significantly varied due to the transmission properties of surrounding objects (i.e., reflection coefficients and penetration losses). This makes the prediction of mmWaves performance very difficult for nLoS. In general, in rural environments, with more trees and vegetation and less buildings, fewer nLoS signal components are generated, which probably is not enough to provide a reliable mmWave link. On the other hand, urban environments, with many buildings made of materials with high

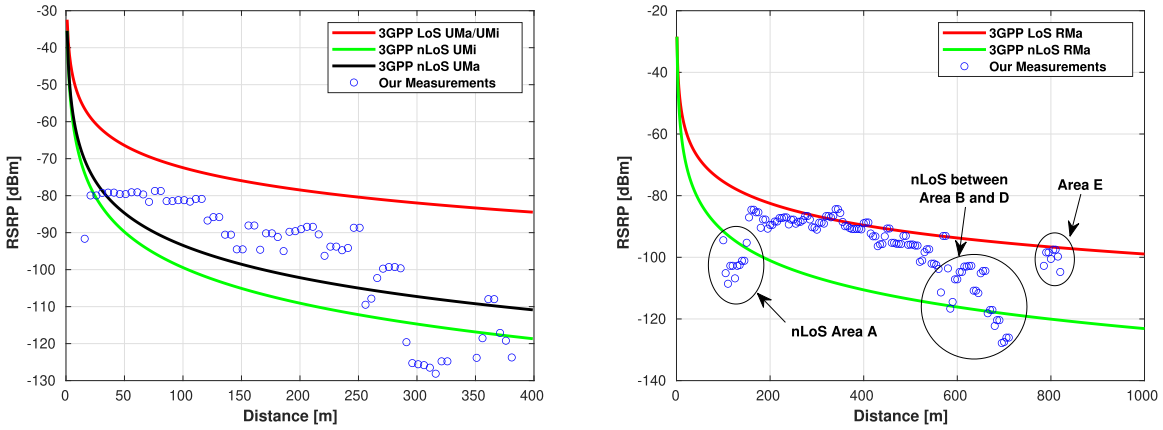

(a) Sector 1 (b) Sector 2

FIGURE 11. Comparing the maximum measured RSRP with simulated 3GPP models for different distances in (a) Sector 1, and (b) Sector 2.

reflection coefficients such as concrete, steel, and glass are more active propagation environments for mmWaves. Hence, nLoS components of the mmWave signals could compensate for the lack of a LoS.

The impact of various environmental phenomena, from rain to foliage, is different on communications over mmWave links. In general, these phenomena can highly degrade the received signal and hence service quality. Regarding the effect of foliage, we observed signal quality drops when the LoS is obstructed by trees, particularly when moved by (even light) wind. However, this generally affects all beams so that the dominant beam remains the same. The measurements have also revealed that wide water surfaces, especially in the presence of waves, can generate time-varying scattering phenomena that affect the stability of the received signal. This is more pronounced if the receiver is higher than the water surface and thus collects more water-reflected waves. The propagation of mmWave on water surfaces is therefore critical and further investigation is required to determine the limitations of links involving floating stations. Comparing the measured RSRP with the simulated omnidirectional (based on 3GPP's path loss models) and strongest RSRP (optimal antenna configuration) shows a considerable gap between the real-world environment and the theoretical performance. This gap could be filled by employing more efficient beamforming techniques.

B. LESSONS LEARNED AND RECOMMENDATIONS FOR VERTICALS

The take-home message for network planners deploying 5G mmWave solutions for applications like forest surveillance and monitoring systems, fish-farm monitoring systems, harbor based ship-hull inspection systems, and anti-grounding services [43] is that deploying a system based on 5G mmWaves needs careful design. Ignoring some environmental factors like rain or wind can significantly affect the system performance.

Our results recommend against employing 5G mmWave in nLoS and dynamic environments (where the LoS link is constantly blocked), at least with current TCP protocols and for applications that require reliable transmissions. Some examples of these use cases are large industrial environments, where LoS links get blocked by hefty mobile machinery, and cell phones, where the antennas can easily be covered and blocked by the user's hands, head, and body. For these cases, combining 5G mmWave with multi-path TCP [23] or TCP proxy architecture [44] can provide better service levels. One interesting use case for 5G mmWave networks that network operators have recently considered is FWA, which aims to provide high-speed Internet for houses, especially in rural environments. Typically, this product is installed at a fixed location at the customers' premises, providing the best possible connectivity to the BS, often with LoS. Internet providers can highly benefit from this solution, as it can decrease costs by replacing the expensive optical fibers with 5G mmWave links. Verticals should consider supplementing theoretical models with on-site measurements to predict cell coverage accurately and identify coverage holes, especially in complex nLoS environments. Solutions that require very high data rates can considerably increase the quality of the received signal at the receiver and hence improve the service rate by employing more efficient beamformers and utilizing the beamforming gain. Also, more advanced beam-tracking or beam-switching techniques should be employed for solutions that require mobility, as the signal strength can drop rapidly by relocating the receiver.

VII. CONCLUSION

Our empirical analysis of a commercial 5G cellular system has confirmed the validity of previous studies carried out on prototypal or PoC deployments or via simulations. Clearly, general theoretical models cannot perfectly capture the complexity of real installments, and significant deviations between model predictions and real-world measurements

have been observed in certain cases. This suggests that the implementation of self-tuning capabilities on commercial installations will be required to adapt the BS configuration to the specificities of the environments, though a first, rough performance estimate can be done using the theoretical models. The effects of body blockage, rain, and trees on the propagation of mmWave signals previously reported in the literature have been mostly reproduced also in our study. This confirms that a commercial version of the mmWave communication interface does not show any significant limitation relative to pre-commercial versions, which was not guaranteed. On the other hand, it does not bring any improvement either. Finally, we noticed that beam selection in a real commercial setting is likely less critical than feared, since the strongest beam appears to remain rather stable in time and space and in bad weather conditions. Therefore beam swiping techniques should be able to track the best beam direction rather easily.

The above observations should help interested stakeholders make more informed decisions when deploying 5G solutions utilizing the mmWave spectrum. Our next steps involve testing verticals' use cases at the same cell site to check if their service requirements are met.

For future works, we will extend the result for the end-to-end transmission study, investigating the performance of TCP variants over unreliable mmWave links in various scenarios. We will also investigate the performance of delay-sensitive applications such as live broadcasting (i.e. a special case of online video streaming) and networked music over 5G networks. Finally, some of the mentioned scenarios can be repeated over operational networks in different customer sites like fish farms, factories, etc.

LIST OF ACRONYMS

3GPP	3rd Generation Partnership Project
5G	5th Generation
BS	Base Station
DKED	Double Knife Edge Diffraction
DTMKE	Double-truncated Multiple Knife-edge
FWA	Fixed Wireless Access
LoS	Line-of-Sight
LTE	Long Term Evolution
mmWave	millimeter wave
nLoS	Non-Line-of-Sight
NSA	Non Standalone
PCI	Physical Cell Identity
PoC	Proof of Concept
QoE	Quality of Experience
RE	Resource Element
RMa	Rural Macro
RSRP	Reference Signal Received Power
RTT	Round Trip Time
SS-RSRP	Synchronization Signal Reference Signal Received Power
SS	Synchronization Signal
SSB	Synchronization Signal Block
SSS	Secondary Synchronization Signal
TCP	Transmission Control Protocol
UE	User Equipment
UMa	Urban Macro
UMi	Urban Micro

REFERENCES

[1] A. Narayanan, E. Ramadan, J. Carpenter, Q. Liu, Y. Liu, F. Qian, and Z.-L. Zhang, "A first look at commercial 5G performance on smartphones," in *Proc. Web Conf.*, Apr. 2020, pp. 894–905.

[2] A. Narayanan, X. Zhang, R. Zhu, A. Hassan, S. Jin, X. Zhu, X. Zhang, D. Rybkin, Z. Yang, Z. M. Mao, F. Qian, and Z.-L. Zhang, "A variegated look at 5G in the wild: Performance, power, and QoE implications," in *Proc. ACM SIGCOMM Conf.*, Aug. 2021, pp. 610–625.

[3] A. Narayanan, E. Ramadan, R. Mehta, X. Hu, Q. Liu, R. A. Fezeu, U. K. Dayalan, S. Verma, P. Ji, T. Li, and F. Qian, "Lumos5G: Mapping and predicting commercial mmWave 5G throughput," in *Proc. ACM Internet Meas. Conf.*, 2020, pp. 176–193.

[4] F. Michelinakis, A. S. Al-Selwi, M. Capuzzo, A. Zanella, K. Mahmood, and A. Elmokashfi, "Dissecting energy consumption of NB-IoT devices empirically," *IEEE Internet Things J.*, vol. 8, no. 2, pp. 1224–1242, Jan. 2021.

[5] *D5.2: Initial Solution and Verification of Aquaculture Use Case Trials*, 5G-HEART Consortium, 2020. [Online]. Available: https://5gheart.org/wp-content/uploads/5G-HEART_D5.2.pdf

[6] *Vertical Industry Use Cases and Requirements in 5G-VINNI.* Accessed: Dec. 19, 2022. [Online]. Available: http://www.6gsummit.com/wp-content/uploads/2019/04/Day2_Session9_Groensund_Telenor.pdf

[7] A. Kaloxylos, A. Gavras, and R. De Peppe, "Empowering vertical industries through 5G networks—Current status and future trends," 5GPPP Technol. Board 5G IA Verticals Task Force, Tech. Rep., Aug. 2020, doi: 10.5281/ZENODO.3698113.

[8] D. Pimienta-Del-Valle, L. Mendo, J. M. Riera, and P. Garcia-Del-Pino, "Indoor LOS propagation measurements and modeling at 26, 32, and 39 GHz millimeter-wave frequency bands," *Electronics*, vol. 9, no. 11, p. 1867, Nov. 2020.

[9] M. Khalily, S. Taheri, S. Payami, M. Ghoraishi, and R. Tafazolli, "Indoor wideband directional millimeter wave channel measurements and analysis at 26 GHz, 32 GHz, and 39 GHz," *Trans. Emerg. Telecommun. Technol.*, vol. 29, no. 10, p. e3311, Oct. 2018.

[10] Z. Lin, X. Du, H.-H. Chen, B. Ai, Z. Chen, and D. Wu, "Millimeter-wave propagation modeling and measurements for 5G mobile networks," *IEEE Wireless Commun.*, vol. 26, no. 1, pp. 72–77, Feb. 2019.

[11] X. Zhao, S. Li, Q. Wang, M. Wang, S. Sun, and W. Hong, "Channel measurements, modeling, simulation and validation at 32 GHz in outdoor microcells for 5G radio systems," *IEEE Access*, vol. 5, pp. 1062–1072, 2017.

[12] J. Ko, Y.-J. Cho, S. Hur, T. Kim, J. Park, A. F. Molisch, K. Haneda, M. Peter, D.-J. Park, and D.-H. Cho, "Millimeter-wave channel measurements and analysis for statistical spatial channel model in in-building and urban environments at 28 GHz," *IEEE Trans. Wireless Commun.*, vol. 16, no. 9, pp. 5853–5868, Jun. 2017.

[13] S. Hur, H. Yu, J. Park, W. Roh, C. U. Bas, R. Wang, and A. F. Molisch, "Feasibility of mobility for millimeter-wave systems based on channel measurements," *IEEE Commun. Mag.*, vol. 56, no. 7, pp. 56–63, Jul. 2018.

[14] P. Zhang, B. Yang, C. Yi, H. Wang, and X. You, "Measurement-based 5G millimeter-wave propagation characterization in vegetated suburban macrocell environments," *IEEE Trans. Antennas Propag.*, vol. 68, no. 7, pp. 5556–5567, Jul. 2020.

[15] C. U. Bas, R. Wang, S. Sangodoyin, S. Hur, K. Whang, J. Park, J. Zhang, and A. F. Molisch, "28 GHz microcell measurement campaign for residential environment," in *Proc. IEEE Global Commun. Conf. (GLOBECOM)*, Dec. 2017, pp. 1–6.

[16] J. Ko, Y.-S. Noh, Y.-C. Kim, S. Hur, S.-R. Yoon, D. Park, K. Whang, D.-J. Park, and D.-H. Cho, "28 GHz millimeter-wave measurements and models for signal attenuation in vegetated areas," in *Proc. 11th Eur. Conf. Antennas Propag. (EUCAP)*, Mar. 2017, pp. 1808–1812.

[17] U. T. Virk and K. Haneda, "Modeling human blockage at 5G millimeter-wave frequencies," *IEEE Trans. Antennas Propag.*, vol. 68, no. 3, pp. 2256–2266, Mar. 2020.

[18] A. Alammouri, J. Mo, B. L. Ng, J. C. Zhang, and J. G. Andrews, "Hand grip impact on 5G mmWave mobile devices," *IEEE Access*, vol. 7, pp. 60532–60544, 2019.
[19] J. Huang, Y. Cao, X. Raimundo, A. Cheema, and S. Salous, "Rain statistics investigation and rain attenuation modeling for millimeter wave short-range fixed links," *IEEE Access*, vol. 7, pp. 156110–156120, 2019.
[20] A. M. Al-Saman, M. Cheffena, M. Mohamed, M. H. Azmi, and Y. Ai, "Statistical analysis of rain at millimeter waves in tropical area," *IEEE Access*, vol. 8, pp. 51044–51061, 2020.
[21] R. Poorzare and A. Calveras, "Open trends on TCP performance over urban 5G mmWave networks," in *Proc. 17th ACM Symp. Perform. Eval. Wireless Ad Hoc, Sensor, Ubiquitous Netw.*, Nov. 2020, pp. 85–92.
[22] R. Poorzare and A. C. Augé, "Challenges on the way of implementing TCP over 5G networks," *IEEE Access*, vol. 8, pp. 176393–176415, 2020.
[23] M. Polese, R. Jana, and M. Zorzi, "TCP and MP-TCP in 5G mmWave networks," *IEEE Internet Comput.*, vol. 21, no. 5, pp. 12–19, Sep. 2017.
[24] M. Polese, R. Jana, and M. Zorzi, "TCP in 5G mmWave networks: Link level retransmissions and MP-TCP," in *Proc. IEEE Conf. Comput. Commun. Workshops (INFOCOM WKSHPS)*, May 2017, pp. 343–348.
[25] M. Zhang, M. Polese, M. Mezzavilla, J. Zhu, S. Rangan, S. Panwar, and M. Zorzi, "Will TCP work in mmWave 5G cellular networks?" *IEEE Commun. Mag.*, vol. 57, no. 1, pp. 65–71, Jan. 2019.
[26] Y. Ren, W. Yang, X. Zhou, H. Chen, and B. Liu, "A survey on TCP over mmWave," *Comput. Commun.*, vol. 171, pp. 80–88, Apr. 2021.
[27] G. R. MacCartney, S. Deng, S. Sun, and T. S. Rappaport, "Millimeter-wave human blockage at 73 GHz with a simple double knife-edge diffraction model and extension for directional antennas," in *Proc. IEEE 84th Veh. Technol. Conf. (VTC-Fall)*, Sep. 2016, pp. 1–6.
[28] Rohde & Schwarz. (2020). *Autonomous Mobile Network Scanner User Manual*. Accessed: Sep. 17, 2021. [Online]. Available: https://www.rohde-schwarz.com/cz/manual/r-stsma6-autonomous-mobile-network-scanner-user-manual-manualsgb1_78701-572421.html
[29] *NR; Physical Layer Measurements (Release 16)*, document TS 38.215, V16.1.0, 3GPP, Mar. 2020.
[30] *Technical Specification Group Radio Access Network; NR; User Equipment (UE) Procedures in Idle Mode and RRC Inactive State*, 3rd Generation Partnership Project (3GPP), Technical Specification, document TS 38.304, Version 16.3.0, 3GPP, Dec. 2020, [Online]. Available: https://portal.3gpp.org/desktopmodules/Specifications/SpecificationDetails.aspx?specificationId=3192
[31] A. Klautau, N. Gonzalez-Prelcic, and R. W. Heath, "LIDAR data for deep learning-based mmWave beam-selection," *IEEE Wireless Commun. Lett.*, vol. 8, no. 3, pp. 909–912, Jun. 2019.
[32] J. Zhu, D. Li, H. Zhao, X. Wang, and R. Jiang, "Adaptive SVM-based beam allocation for mmWave small cell networks," in *Proc. Int. Conf. Wireless Commun. Signal Process. (WCSP)*, Oct. 2020, pp. 558–562.
[33] *Study on Channel Model for Frequencies From 0.5 to 100 GHz*, 3rd Generation Partnership Project (3GPP), document TR 38.901, Version 16.1.0, 3GPP, Jan. 2020, [Online]. Available: https://portal.3gpp.org/desktopmodules/Specifications/SpecificationDetails.aspx?specificationId=3173
[34] H. M. Rahim, C. Y. Leow, T. A. Rahman, A. Arsad, and M. A. Malek, "Foliage attenuation measurement at millimeter wave frequencies in tropical vegetation," in *Proc. IEEE 13th Malaysia Int. Conf. Commun. (MICC)*, Nov. 2017, pp. 241–246.
[35] M. Lecci, M. Polese, C. Lai, J. Wang, C. Gentile, N. Golmie, and M. Zorzi, "Quasi-deterministic channel model for mmWaves: Mathematical formalization and validation," in *Proc. IEEE Global Commun. Conf. (GLOBECOM)*, Dec. 2020, pp. 1–6.
[36] N. Varshney, J. Wang, C. Lai, C. Gentile, R. Charbonnier, and Y. Corre, "Quasi-deterministic channel propagation model for an urban environment at 28 GHz," *IEEE Antennas Wireless Propag. Lett.*, vol. 20, no. 7, pp. 1145–1149, Jul. 2021.
[37] *LTE; 5G; Study on Channel Model for Frequency Spectrum Above 6 GHz (3GPP TR 38.900 Version 14.2.0 Release 14)*, document TR 138 900, V14.2.0, 2017. [Online]. Available: https://portal.etsi.org/TB/ETSIDeliverableStatus.aspx
[38] K. Haneda, J. Zhang, L. Tan, G. Liu, Y. Zheng, H. Asplund, J. Li, Y. Wang, D. Steer, C. Li, and T. Balercia, "5G 3GPP-like channel models for outdoor urban microcellular and macrocellular environments," in *Proc. IEEE 83rd Veh. Technol. Conf.*, May 2016, pp. 1–7.
[39] G. R. MacCartney, M. K. Samimi, and T. S. Rappaport, "Omnidirectional path loss models in New York city at 28 GHz and 73 GHz," in *Proc. IEEE 25th Annu. Int. Symp. Pers., Indoor, Mobile Radio Commun. (PIMRC)*, Sep. 2014, pp. 227–231.
[40] G. R. MacCartney and T. S. Rappaport, "Rural macrocell path loss models for millimeter wave wireless communications," *IEEE J. Sel. Areas Commun.*, vol. 35, no. 7, pp. 1663–1677, Jul. 2017.
[41] S. Sun, G. R. MacCartney, and T. S. Rappaport, "A novel millimeter-wave channel simulator and applications for 5G wireless communications," in *Proc. IEEE Int. Conf. Commun. (ICC)*, May 2017, pp. 1–7.
[42] S. Ju, O. Kanhere, Y. Xing, and T. S. Rappaport, "A millimeter-wave channel simulator NYUSIM with spatial consistency and human blockage," in *Proc. IEEE Global Commun. Conf. (GLOBECOM)*, Dec. 2019, pp. 1–6.
[43] D. Zordan, F. Campagnaro, and M. Zorzi, "On the feasibility of an anti-grounding service with autonomous surface vessels," in *Proc. OCEANS Marseille*, Jun. 2019, pp. 1–8.
[44] M. Polese, M. Mezzavilla, M. Zhang, J. Zhu, S. Rangan, S. Panwar, and M. Zorzi, "MilliProxy: A TCP proxy architecture for 5G mmWave cellular systems," in *Proc. 51st Asilomar Conf. Signals, Syst., Comput.*, Oct. 2017, pp. 951–957.

SALMAN MOHEBI (Member, IEEE) received the M.Sc. degree in information technology from the University of Tehran, Iran, in 2017. He is currently pursuing the Ph.D. degree with the Department of Information Engineering, University of Padova, Italy. In 2022, he was a Visiting Scholar at the Telenor Research, Fornebu, Norway, and the Swiss Data Science Center (SDSC), ETH, Zurich, Switzerland. He is a Marie Skłodowska-Curie ESR Fellow involved in the MSCA ITN WinMill Project. His primary research interests include the machine learning applications in different wireless networks, including mmWaves and cell-free massive MIMO networks.

FOIVOS MICHELINAKIS (Member, IEEE) received the master's degree in telematics from University Carlos III of Madrid, the Engineering Diploma degree in electrical engineering from National Technical University of Athens, and the Ph.D. degree in optimizing the delivery of multimedia over mobile networks from the IMDEA Networks Institute and University Carlos III of Madrid, in September 2018. He is currently a Research Scientist with the Simula Metropolitan, working on verification and validation of commercial and testbed 5G deployments and usecases. His research interests include mobile networks, network optimization, and content distribution networks.

AHMED ELMOKASHFI (Member, IEEE) received the Ph.D. degree from the University of Oslo, in 2011. He is currently as Research Professor with the Simula Metropolitan Centre for Digital Engineering, Norway. He is currently the Heading of the Centre for Resilient Networks and Applications (CRNA), which is part of the Simula Metropolitan Centre that is funded by the Norwegian Ministry of Transport and Communication. His research interest includes network measurements and performance. In particular, he has been focusing on studying the resilience, scalability, and evolution of the internet infrastructure; the measurement and quantification of robustness in mobile broadband networks; and the understanding of dynamical complex systems. Over the past few years, he has been leading and contributing to the development, operation and management the NorNet Testbed Infrastructure, which is a countrywide measurement setup for monitoring the performance of mobile broadband networks in Norway.

OLE GRØNDALEN received the Master of Science degree in physics from the University of Oslo, in 1987, and the Dr.Philos. degree from the Norwegian University of Science and Tecnnology, in 2019. He is currently a Senior Research Scientist with the Telenor Research. His research covers satellite and terrestrial broadcasting systems, fixed broadband wireless access systems, and mobile radio technologies. His current research interests include performance analysis of wireless networks, self-organized networks, and methods for interference control in heterogeneous networks.

KASHIF MAHMOOD received the master's degree in electronics from the GIK Institute, Pakistan, in 2007, and the Ph.D. degree in telematics from the Norwegian University of Science and Technology (NTNU), Norway, in 2012. He has contributed to a number of European research projects. He is currently a Senior Research Scientist with the Telenor Research, Norway. His current research interests include design of next-generation network architecture, performance analysis of wireless networks, and analyzing cellular traffic. He received 1st position in master's degree, the Excellence Award in engineering from the National Engineering and Scientific Commission, Pakistan, and the Youth Award in science in technology from the Government of Pakistan.

ANDREA ZANELLA (Senior Member, IEEE) received the Laurea degree in computer engineering from the University of Padova, Italy, and the Ph.D. degree in 2001. He is currently a Full Professor with the Department of Information Engineering (DEI), University of Padova. In 2000, he was a Visiting Scholar at the University of California, Los Angeles (UCLA), within Prof. Mario Gerla's Research Team. He has long-established research activity is in the field of protocol design, optimization, and performance evaluation of wired and wireless networks. He has authored more than 190 articles. He has been serving in the Editorial Board of several top journals, such as IEEE Internet of Things Journal, IEEE Communications Surveys and Tutorials, and IEEE Transactions on Cognitive Communications and Networking.

Open Access funding provided by 'Università degli Studi di Padova' within the CRUI CARE Agreement